

Charge-density-wave phase, mottness and ferromagnetism in monolayer $1T$ -NbSe₂

Diego Pasquier and Oleg V. Yazyev*

Institute of Physics, Ecole Polytechnique Fédérale de Lausanne (EPFL), CH-1015 Lausanne, Switzerland

(Dated: March 5, 2022)

The recently investigated $1T$ -polymorph of monolayer NbSe₂ revealed an insulating behaviour suggesting a star-of-David phase with $\sqrt{13} \times \sqrt{13}$ periodicity associated with a Mott insulator, reminiscent of $1T$ -TaS₂. In this work, we examine this novel two-dimensional material from first principles. We find an instability towards the formation of an incommensurate charge-density-wave (CDW) and establish the star-of-David phase as the most stable commensurate CDW. The mottness in the star-of-David phase is confirmed and studied at various levels of theory: the spin-polarized generalized gradient approximation (GGA) and its extension involving the on-site Coulomb repulsion (GGA+ U), as well as the dynamical mean-field theory (DMFT). Finally, we estimate Heisenberg exchange couplings in this material and find a weak nearest-neighbour ferromagnetic coupling, at odds with most Mott insulators. We point out the close resemblance between this star-of-David phase and flat-band ferromagnetism models.

I. INTRODUCTION

Transition metal dichalcogenides (TMDs) have been extensively studied for their charge-density-wave phases [1–4], historically being the first materials where the Peierls instability [5] manifests itself, although this point of view has been frequently challenged in the last few years [6, 7]. More recently, TMDs (for recent reviews see e.g. [8, 9]) have further attracted attention due to their novel topological properties [10, 11], unconventional Ising superconductivity [12–15], as well as the possibility to thin them down to a single layer [16], leading to a rich family of two-dimensional (2D) materials that includes semiconductors with promising technological applications [17].

TMDs with chemical composition MX_2 are layered materials, each layer consisting of a transition metal ($M = \text{Ti, V, Nb, Ta, etc.}$) forming a triangular lattice sandwiched between two atomic planes of chalcogen atoms ($X = \text{S, Se, Te}$). The local coordination sphere of the transition metal can have either trigonal prismatic or distorted octahedral symmetry, giving rise to two families of polytopes, referred to as $2H$ and $1T$, respectively, where 1 and 2 stand for the number of inequivalent layers in the unit cell for bulk materials. The different coordination environments lead to distinct crystal field splittings of the d -like bands and therefore very different electronic properties [8].

Among all the TMDs, $1T$ -TaS₂ displays arguably the most complex phase diagram. Indeed, $1T$ -TaS₂ exhibits a series of structural phase transitions, that involves one second-order and two first-order transitions, upon decreasing temperature [2, 18, 19]. The low-temperature commensurate CDW phase is characterized by the formation of star-of-David clusters of Ta atoms in a $\sqrt{13} \times \sqrt{13}$ supercell associated with the emergence of a narrow band crossing the Fermi level [20, 21], favouring the opening of

a Mott correlation gap. Moreover, it has recently been pointed out that no trace of magnetic order is observed down to very low temperatures, indicating a possible quantum spin liquid (QSL) state [22].

Only known so far in the $2H$ phase, $1T$ -NbSe₂ has recently been successfully synthesized in a monolayer form [23]. Niobium is situated in the same column of the periodic table as Tantalum, which implies that these two transition metal elements are isoelectronic and have formal d -shell populations of $4d^1$ and $5d^1$ in NbSe₂ and TaS₂, respectively. It has been found that a superlattice is formed in monolayer $1T$ -NbSe₂ and that the electronic structure exhibits an insulating energy gap of ~ 0.4 eV, strongly suggesting a phase diagram analogous to $1T$ -TaS₂.

The purpose of this paper is to provide a first-principles study of this new material, including the instability of the metallic undistorted $1T$ phase towards a CDW phase, structural properties and different scenarios for the nature of the gap, correlation effects and magnetism. Our work confirms the $\sqrt{13} \times \sqrt{13}$ phase as the most stable commensurate CDW phase as well as the opening of a correlation gap that is to some extent captured even by spin-polarized GGA calculations. GGA+ U and GGA+DMFT calculations provide further insight and suggest a gap of the charge transfer type. An estimation of Heisenberg exchange couplings surprisingly indicates a ferromagnetic ground state, contrary to what one would expect in a Mott insulator. We suggest that, if confirmed, the ferromagnetism strongly resembles the flat-band ferromagnetism [24–31] effect in multiband Hubbard models and that this star-of-David phase could be a real material realization of this effect in 2D.

This paper is organized as follows. Section II briefly describes the computational methodology. In Section III, we study the fermiology and the phonon dispersion of the undistorted $1T$ phase, as well as possible commensurate superlattices. In Sections IV and V, we present an analysis of the electronic structure and magnetism of the $\sqrt{13} \times \sqrt{13}$ phase. Section VI offers conclusions.

* E-mail: oleg.yazyev@epfl.ch

II. COMPUTATIONAL METHODOLOGY

First-principles density functional theory (DFT) calculations were performed using the QUANTUM ESPRESSO package [32]. The interaction between the valence and core electrons is described by means of ultrasoft pseudopotentials [33] (available from the PSLIBRARY [34, 35]), explicitly including the s and p semi-core electrons as valence electrons for Nb atoms. The plane-wave cutoffs are set to 60 and 300 Ry for the wave functions and charge density, respectively. The exchange-correlation functional is approximated by the generalized gradient approximation according to Perdew, Burke and Ernzerhof (PBE) [36]. For GGA+ U calculations, we adopt the simplified formulation of Cococcioni and de Gironcoli [37], with a Hubbard parameter $U = 3.02$ eV for Nb $4d$ orbitals, calculated from linear response in a supercell of the undistorted $1T$ phase containing 75 atoms. Brillouin zone integration is performed on a $24 \times 24 \times 1$ k-points mesh ($8 \times 8 \times 1$ and $6 \times 6 \times 1$ for the $\sqrt{13} \times \sqrt{13}$ and 4×4 supercells, respectively) and a Marzari-Vanderbilt smearing [38] of 1 mRy. To simulate the monolayer form, we include approximately 13 Å of vacuum between periodic replicas. Lattice constants and atomic positions of various phases are determined by fully relaxing the structure at the PBE level until all the Hellmann-Feynman forces are less than 10^{-4} Ry/Bohr. The spin-orbit coupling is not included but its effect is described in the Supplementary information document [39].

The phonon dispersion is calculated within density functional perturbation theory (DFPT) [40], using a denser mesh of $84 \times 84 \times 1$ k-points and a larger smearing of 5 mRy. To plot the full dispersion, we have calculated the phonons on a 12×12 grid of q-points and used Fourier interpolation. In addition, we have computed the dispersion close to the CDW wave vector by performing a DFPT calculation for several points in its vicinity, using different smearings of 10 mRy, 5 mRy and 2.5 mRy and a denser grid of 192×192 k-points to ensure convergence of the imaginary frequencies.

Dynamical mean-field theory (DMFT) [41] calculations are performed using the AMULET code [42]. The quantum impurity problem is solved with the continuous-time quantum Monte-Carlo (CT-QMC) algorithm [43] with ten millions QMC steps. The simplified fully localized limit prescription is adopted to account for double counting. The spectrum is obtained with the maximum entropy method.

Maximally localized Wannier functions (MLWF) [44, 45] are obtained using the WANNIER90 code [46]. The susceptibility is calculated on a dense $400 \times 400 \times 1$ k-points grid with Wannier-interpolated bands.

III. CHARGE-DENSITY-WAVE PHASES

We begin our discussion by determining the structural and electronic properties of the undistorted $1T$

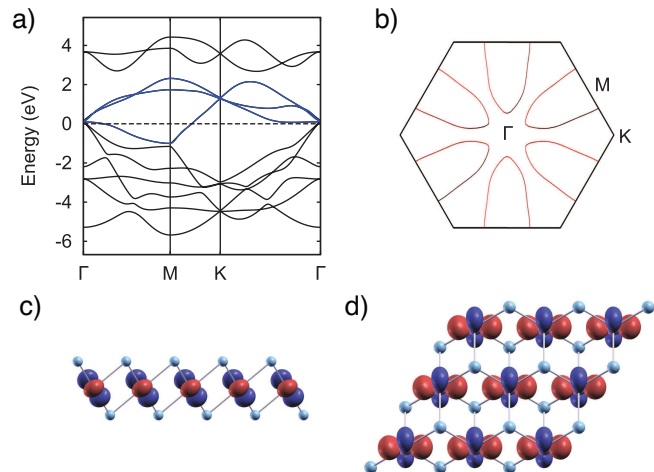


FIG. 1. (a) GGA band structure of the undistorted $1T$ -phase of monolayer NbSe₂. The t_{2g} bands are emphasized in blue. The dashed line corresponds to the Fermi energy, set to zero. (b) Fermi surface of monolayer NbSe₂. (c),(d) Ball-and-stick representation of the undistorted $1T$ phase of monolayer NbSe₂ with an isosurface plot of one of the three symmetry-equivalent t_{2g} -like Wannier functions. Selenium atoms are shown in blue.

polymorph of monolayer NbSe₂. The latter contains three atoms per unit cell and belongs to the symmorphic D_{3d}^3 space group. The lattice constant and the Nb–Se distance at the PBE level are $a = 3.49$ Å and $d_{\text{Nb-Se}} = 2.62$ Å, respectively.

The electronic structure and the t_{2g} Fermi surface are shown in Figure 1. Since the spin-orbit coupling does not play an important role, we neglect it but briefly describe its effect in the Supplementary material [39]. The three t_{2g} bands are filled with one electron. The bandwidth is rather large (~ 3 eV), implying that the moderate electron-electron interactions can be neglected at this point. On the other hand, the t_{2g} electrons are prone to form σ -bonds due to their directional character, implying a large coupling to a local bond-stretching phonon. The latter is, to the best of our understanding, responsible for the recurrent occurrence of CDWs in the $1T$ dichalcogenides and lead to stronger distortions when the filling is closer to half-filling, as e.g. in $1T'$ -MoS₂ [47] or ReS₂ [48], in which strong metal-metal bonds are formed. The Fermi surface is typical of group V $1T$ dichalcogenides and displays pseudo-nesting, favouring density wave instabilities with incommensurate wave vectors $\mathbf{Q}_i = Q_{\text{ICDW}}\mathbf{b}_i$, where \mathbf{b}_i ($i = 1, 2, 3$) are the three reciprocal lattice vectors of a triangular lattice and $Q_{\text{ICDW}} \approx 0.25 - 0.33$ [2, 49], depending on material-dependent details of the electronic structure.

Figure 2 shows the calculated phonon dispersion curves and bare static susceptibility along the $\Gamma - M$ direction.

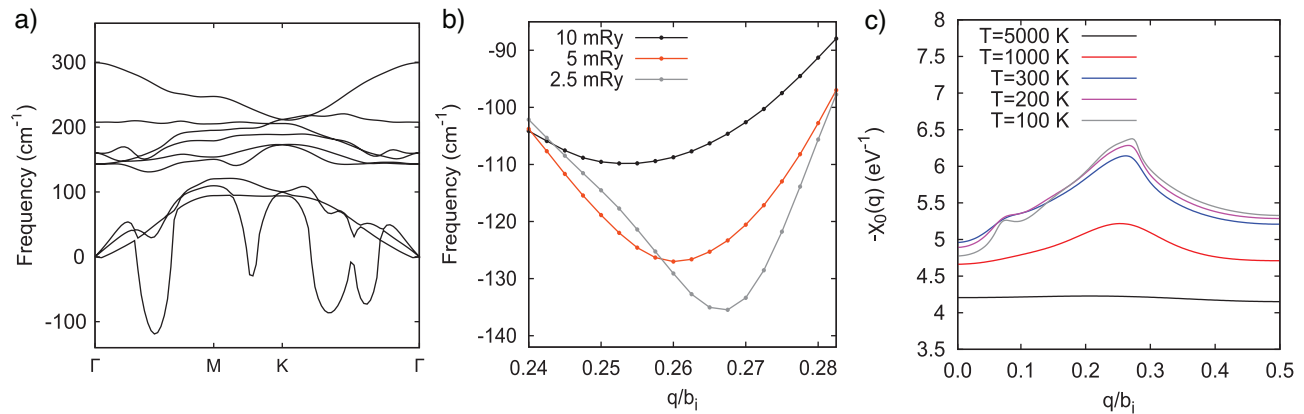


FIG. 2. (a) Calculated phonon dispersion for the undistorted $1T$ phase of monolayer NbSe_2 obtained by Fourier interpolation. Imaginary frequencies are plotted as negative. (b) Phonon dispersion close to the wave vector of maximum softening with different electronic population smearing values. Each point corresponds to a DFPT calculation. (c) Calculated bare static susceptibility along the $\Gamma - M$ direction at different electronic temperatures.

Neglecting matrix elements, the susceptibility reads

$$\chi_0(q) = \frac{1}{N_k} \sum_{k,n,m} \frac{f(\epsilon_{n,k+q}) - f(\epsilon_{m,k})}{\epsilon_{n,k+q} - \epsilon_{m,k}}, \quad (1)$$

where $f(\epsilon_{n,k})$ is the Fermi-Dirac distribution and $\epsilon_{n,k}$ are the Kohn-Sham energies. The susceptibility is proportional to the phonon self-energy in the random phase approximation, favouring soft phonon modes when it is enhanced at a particular wave vector [50]. One can see that the system is unstable against the formation of a CDW with momentum $Q_{\text{ICDW}} \approx 0.26$, corresponding to the maximum of the susceptibility at $T = 300$ K (Fig. 2b). At lower temperatures, the maximum is shifted closer to $Q_{\text{ICDW}} = 0.27$. Accordingly, the calculated phonon softening becomes stronger closer to $Q_{\text{ICDW}} = 0.27$ when a smaller smearing is used. We also observe that at $T = 5000$ K the susceptibility is completely flat as the Fermi surface is blurred. The incommensurability of the soft phonon mode and its correlation with the maximum of the susceptibility demonstrate the effect of the fermiology on the CDW (Fig. 2c), even if we stress that the latter is possible only in the presence of a rather strong electron-phonon coupling due to imperfect nesting.

As understood by McMillan [51, 52], density waves can further gain energy by adopting a commensurate periodicity characterized by a momentum Q_{CCDW} close to Q_{ICDW} . This can lead to first-order incommensurate-to-commensurate phase transitions (lock-in transitions) as the temperature is lowered. Such transitions come from higher-order terms of the free energy and are therefore not captured by a phonon calculation. The calculated $Q_{\text{ICDW}} \approx 0.26$ suggests either 4×4 or $\sqrt{13} \times \sqrt{13}$ periodicity. In the latter case, each unit cell contains an odd number of electrons and an insulating gap, as observed in experiments, can only come from electron correlations. On the other hand, the 4×4 cell could possibly be a normal band insulator. We have therefore addressed both

scenarios by relaxing atomic positions (starting from randomized ones) and lattice vectors in the two supercells.

For the 4×4 cell, we obtain an energy gain of 49 meV per NbSe_2 formula unit compared to the undistorted $1T$ phase and a magnetically ordered metallic phase (see supplementary information [39]), whereas for the $\sqrt{13} \times \sqrt{13}$ cell we obtain the star-of-David phase with a larger energy gain of 69 meV/f.u. and a Mott insulator phase (see next section). Another possibility would be that the CDW remains incommensurate down to zero temperature. However, incommensurate CDWs in the dichalcogenides usually have a rather small effect on the electronic structure so that it is unlikely that a gap of ~ 0.4 eV could be opened.

IV. MOTTNES IN THE STAR-OF-DAVID PHASE

We now proceed to study the electronic structure of the star-of-David phase at various levels of theory. As one can see in Figure 3a, a very narrow band crossing the Fermi level emerges in the GGA band structure. Spin-polarized GGA already captures some correlation effects and can sometimes describe mottness approximately (but not in quantitative agreement with experiments [53]), together with a magnetic solution. In Figure 3b, we observe a small band gap of ~ 20 meV at the spin-polarized GGA level with a total magnetic moment of $1 \mu_B$ per supercell that contains one David star. The computed gap is clearly too small compared to the experiments, therefore we add an on-site Hubbard repulsion $U = 3.02$ eV for Nb $4d$ orbitals. The calculated gap is now ~ 0.3 eV (Fig. 3c), in better agreement with the experimental data. However, the gap appears to be between the "uncorrelated" bands rather than between the lower Hubbard band (LHB) and the upper Hubbard band (UHB), as expected in Ref. 23. We note that the flat LHB

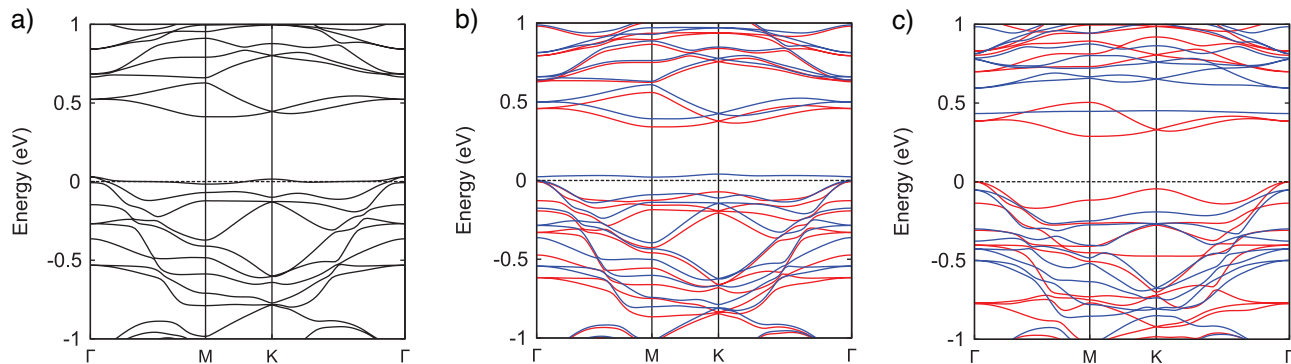


FIG. 3. (a) Electronic band structure of the $\sqrt{13} \times \sqrt{13}$ CCDW phase of monolayer NbSe₂ obtained from non-spin-polarized GGA calculations. The dashed line corresponds to the Fermi level, set to zero. (b),(c) Electronic band structures obtained from spin-polarized (b) GGA and (c) GGA+ U ($U = 3.02$ eV) calculations. The up and down spin bands are shown in red and blue, respectively.

and UHB bands can still be distinguished amongst the "uncorrelated" bands in Fig. 3c.

To gain further insight, we derive a minimal three-bands (occupied by five electrons) tight-binding model in the basis of maximally localized Wannier functions. We obtain, as can be seen on Figure 4, one Wannier function (type I WF) localized at the center of the star with a spread of 22 \AA^2 , giving rise to the narrow band and two Wannier functions (type II WFs, see Supplementary information [39]) with larger spreads and more weights on the outer Nb atoms of the David stars, hybridizing very weakly with the type I WF. This choice of model allows to capture the bands crossing the Fermi level and to disentangle the narrow "correlated" band, constituting therefore a minimal model to understand the opening of a correlation gap. Treating only the type I WF as correlated with a single variable on-site Hubbard parameter U , we solve the model with DMFT in the paramagnetic phase with an inverse temperature of 40 eV^{-1} ($T \approx 300 \text{ K}$).

Since the band derived from type I WFs is nearly flat with a bandwidth of $\sim 30 \text{ meV}$, it splits into a LHB and a UHB upon any small interaction, explaining why the GGA functional can already capture the gap opening. With a sufficiently large Hubbard U , a gap opens between the type II bands and the UHB (charge transfer insulator) and the orbital population of the type I WF changes from 1.18 in GGA to 1.0 in GGA+DMFT. A Hubbard parameter $U \sim 0.9 \text{ eV}$ gives a gap between the type II bands and the UHB consistent with the GGA+ U calculation. Obviously, the U parameter for the type I WF is expected to be smaller than that for the Nb $4d$ orbitals in GGA+ U due to a larger spread.

We note that in the GGA+ U band structure (Fig. 3c), while a flat UHB is easily recognizable, the LHB appears to further hybridize with other bands, even if a flat-like band is seen at $\sim 0.5 \text{ eV}$ below the valence band maximum. This suggests that it would be interesting to compare this minimal three-bands models with more elaborate models containing more bands and to take into

account charge self-consistency, but this is beyond the scope of the present work.

V. MAGNETIC PHASES

In Mott insulators, the low-energy degrees of freedom are localized spins whose interactions lead to long-range magnetic order below a characteristic temperature, unless prevented by strong fluctuations (i.e. a QSL state). It is therefore natural to study the mean-field magnetic solutions obtained from DFT to anticipate the character of magnetic correlations expected in a material.

In Figure 5, we present an isovalue plot of the spin polarization density obtained from the GGA+ U calculations. While the total magnetic moment is $1 \mu_B$ per star-of-David ($S = 1/2$ Mott insulator), the absolute magnetization is found close to $3\mu_B/\text{star}$. This is an effect of the on-site Hubbard repulsion, since in the GGA case, the latter is close to one ($1.19 \mu_B/\text{star}$). In the GGA+ U solution, the Nb atom at the center of the star acquires a larger magnetic moment (0.8 against $0.2 \mu_B$), while its six nearest-neighbours Se atoms, as well as the six outer Nb atoms, acquire small opposite magnetic moments, as can be seen in the spin polarization plot. Our GGA+ U solution therefore bears resemblance with ferrimagnetism. However, we stress that the opposite magnetic moments are the consequence of a spin-splitting of the lower bands induced by the magnetic moment associated with the LHB in GGA+ U . Focusing on the global properties of the system, we address the question whether the total spins on neighbouring stars couple ferromagnetically or antiferromagnetically [53]. We therefore compare the total energies of different spin configurations in the $2\sqrt{13} \times \sqrt{13}$ and $\sqrt{3}\sqrt{13} \times \sqrt{3}\sqrt{13}$ supercells (containing two and three stars per supercell, respectively) to extract effective nearest-neighbour and next-nearest-neighbour Heisenberg exchange couplings J_1 and J_2 , as illustrated in Figure 5, assuming that further couplings can be neglected. We stress that we are aware that DFT

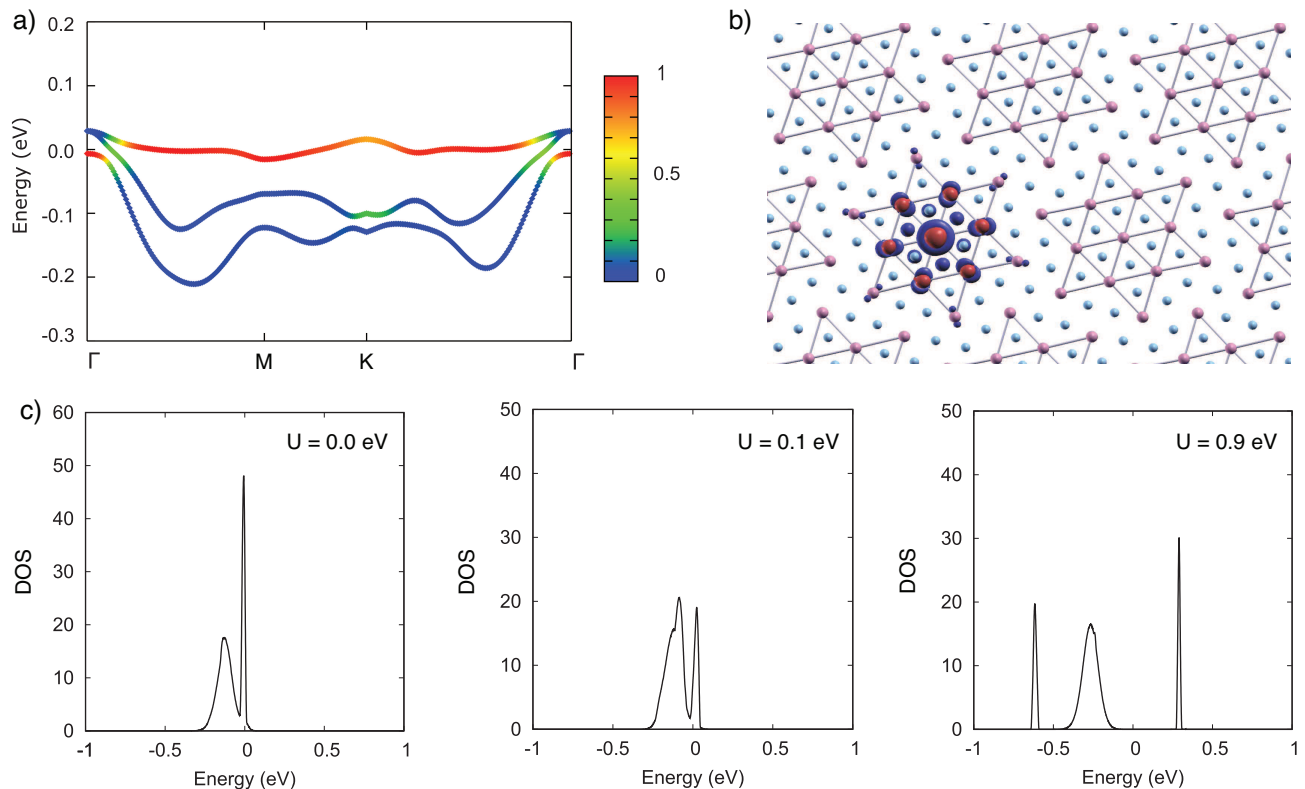


FIG. 4. (a) Three-band model chosen for the DMFT calculations with the orbital weight of the type I Wannier function color-coded. (b) Ball-and-stick representation of the star-of-David phase with an iso-value plot of the type I Wannier function. Nb–Nb bonds are drawn to facilitate the visualization. (c) Spectra obtained by analytic continuation of the imaginary-time Green’s functions for $U = 0.0, 0.1$ and 0.9 eV. The Fermi energy is set to zero.

TABLE I. Calculated nearest-neighbour (J_1) and next-nearest-neighbour (J_2) ferromagnetic exchange couplings in Kelvins.

	J_1 (K)	J_2 (K)
GGA	2.38	0.12
GGA+ U	4.77	0.04

can sometimes give misleading results for magnetic properties, but more accurate wave functions method would be prohibitive for this system and we therefore restrict ourselves to GGA and GGA+ U .

The estimated magnetic exchange couplings are reported in Table I. We find a weak nearest-neighbour ferromagnetic coupling and a negligible next-nearest-neighbour coupling. This is rather unexpected since Mott insulators are usually antiferromagnetic, with a few exceptions such as YTiO_3 [54] or Ba_2NaOs_6 [55]. We have also verified that introducing the spin-orbit coupling does not affect the sign of the magnetic exchange coupling parameters, even though it gives rise to small anisotropies (see the supplementary information [39]). A possible scenario for the occurrence of ferromagnetism in multiband Hubbard models is the so-called flat-band

ferromagnetism studied by Mielke and Tasaki [24–28]. Flat-band ferromagnetism can emerge, for instance, on the Kagome lattice with nearest-neighbour hoppings only [56–58]. While a perfectly flat band requires fine-tuning of the model parameters unlikely to happen in any real material, ferromagnetism is robust against some deviations [31, 57] if the (nearly) flat-band is at half-filling. In the monolayer $1T\text{-NbSe}_2$ case, the flat-band has some dispersion and overlaps in energy with two other bands. Intuitively, the direct antiferromagnetic exchange is expected to be small because the correlated type I Wannier function are at the center of the stars and have hence small direct hoppings. Therefore, higher-order processes can become dominant and ferromagnetic couplings can be enabled depending on the sign of the different hopping parameters. It is expected that several mechanisms are involved, including the effect of the spin polarization of the “uncorrelated” bands, and that a quantitative model would likely be rather complicated.

We point out that monolayer $1T\text{-TaS}_2$ seems even closer to the ideal flat-band model since the narrow band is well isolated. We have verified that in this system the magnetic exchange coupling is also ferromagnetic at the GGA and GGA+ U levels of theory (in agreement with Ref. 59). We stress that this is not in contradiction with the absence of magnetism observed experimen-

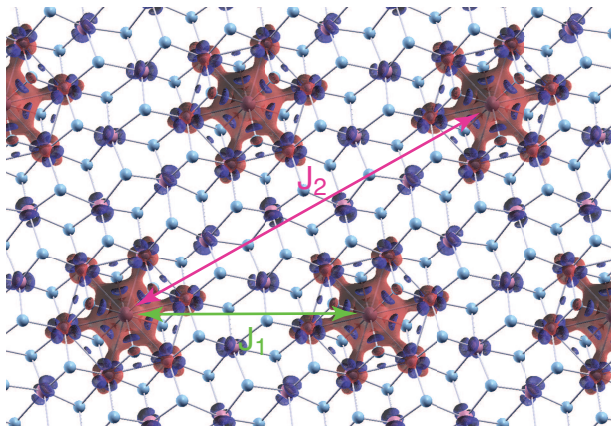


FIG. 5. Spin polarization density in monolayer NbSe₂ obtained at the GGA+*U* level in the ferromagnetic phase. A small isovalue of $0.0025 a_0^{-3}$ was chosen to visualize the opposite polarization on the outer star-of-David atoms. The definitions of nearest-neighbour (J_1) and next-nearest-neighbour (J_2) exchange coupling are indicated.

tally, since all experimental studies of magnetism so far were carried out on bulk materials, for which both experiments and calculations suggest significant dispersion between the layers and the existence of a Fermi surface [20, 59–61]. On the other hand, the ferromagnetic scenario does not seem to agree with the recent proposal of a quasi-2D quantum spin liquid phase in 1*T*-TaS₂ [22], that could occur, e.g. in a J_1 - J_2 antiferromagnetic model on a triangular lattice with $0.08 \leq J_2/J_1 \leq 0.16$ [62]. It would therefore be interesting to address experimentally the possible magnetic ordering in monolayer 1*T*-NbSe₂ and 1*T*-TaS₂ at low temperatures.

VI. CONCLUSIONS

In our work, we addressed by means of first-principles calculations monolayer 1*T*-NbSe₂ that was recently realized experimentally. We found an instability against an incommensurate CDW and established the $\sqrt{13} \times \sqrt{13}$ CCDW with the star-of-David distortion as the most stable phase. Our calculations performed at the level of DFT, DFT+*U* and DMFT identify this configuration as a Mott insulator. Finally, we suggested the possible existence of ferromagnetic ordering in this star-of-David phase and pointed out the resemblance with the so-called flat-band ferromagnetism scenario. The emergence of the narrow band close to the Fermi level in the CCDW phase leads to exotic physics making these materials unique in the family of the TMDs.

ACKNOWLEDGEMENTS

We acknowledge funding by the European Commission under the Graphene Flagship (Grant agreement No. 696656). We thank Hyungjun Lee, QuanSheng Wu and Vamshi Katukuri for useful discussions. First-principles calculations were performed at the Swiss National Supercomputing Centre (CSCS) under project s675 and the facilities of Scientific IT and Application Support Center of EPFL.

Note: While the manuscript was in the final stage of preparation, a related work on monolayer 1*T*-NbSe₂ has been reported [63].

-
- [1] J. A. Wilson, F. J. Di Salvo, and S. Mahajan, *Physical Review Letters* **32**, 882 (1974).
 - [2] J. A. Wilson, F. J. Di Salvo, and S. Mahajan, *Advances in Physics* **24**, 117 (1975).
 - [3] A. H. Castro Neto, *Physical Review Letters* **86**, 4382 (2001).
 - [4] K. Rossnagel, *Journal of Physics: Condensed Matter* **23**, 213001 (2011).
 - [5] R. E. Peierls, *Quantum theory of solids*, 23 (Oxford University Press, 1955).
 - [6] M. D. Johannes and I. I. Mazin, *Physical Review B* **77**, 165135 (2008).
 - [7] X. Zhu, Y. Cao, J. Zhang, E. W. Plummer, and J. Guo, *Proceedings of the National Academy of Sciences* **112**, 2367 (2015).
 - [8] M. Chhowalla, H. S. Shin, G. Eda, L.-J. Li, K. P. Loh, and H. Zhang, *Nature Chemistry* **5**, 263 (2013).
 - [9] S. Manzeli, D. Ovchinnikov, D. Pasquier, O. V. Yazyev, and A. Kis, *Nature Reviews Materials* **2**, 17033 (2017).
 - [10] X. Qian, J. Liu, L. Fu, and J. Li, *Science* **346**, 1344 (2014).
 - [11] A. A. Soluyanov, D. Gresch, Z. Wang, Q. Wu, M. Troyer, X. Dai, and B. A. Bernevig, *Nature* **527**, 495 (2015).
 - [12] J. M. Lu, O. Zheliuk, I. Leermakers, N. F. Q. Yuan, U. Zeitler, K. T. Law, and J. T. Ye, *Science* **350**, 1353 (2015).
 - [13] X. Xi, Z. Wang, W. Zhao, J.-H. Park, K. T. Law, H. Berger, L. Forró, J. Shan, and K. F. Mak, *Nature Physics* **12**, 139 (2016).
 - [14] N. F. Q. Yuan, K. F. Mak, and K. Law, *Physical Review Letters* **113**, 097001 (2014).
 - [15] Y. Saito, Y. Nakamura, M. S. Bahramy, Y. Kohama, J. Ye, Y. Kasahara, Y. Nakagawa, M. Onga, M. Tokunaga, T. Nojima, Y. Yanase, and Y. Iwasa, *Nature Physics* **12**, 144 (2016).
 - [16] K. S. Novoselov, D. Jiang, F. Schedin, T. J. Booth, V. V. Khotkevich, S. V. Morozov, and A. K. Geim, *Proceedings of the National Academy of Sciences of the United States of America* **102**, 10451 (2005).
 - [17] Q. H. Wang, K. Kalantar-Zadeh, A. Kis, J. N. Coleman, and M. S. Strano, *Nature nanotechnology* **7**, 699 (2012).
 - [18] F. J. Di Salvo and J. E. Graebner, *Solid State Communications* **23**, 825 (1977).
 - [19] B. Sipos, A. F. Kusmartseva, A. Akrap, H. Berger,

- L. Forró, and E. Tutiš, *Nature Materials* **7**, 960 (2008).
- [20] P. Darancet, A. J. Millis, and C. A. Marianetti, *Physical Review B* **90**, 045134 (2014).
- [21] T. Ritschel, J. Trinckauf, K. Koepf, B. Büchner, M. v. Zimmermann, H. Berger, Y. I. Joe, P. Abbamonte, and J. Geck, *Nature Physics* **11**, 328 (2015).
- [22] K. T. Law and P. A. Lee, *Proceedings of the National Academy of Sciences* **114**, 6996 (2017).
- [23] Y. Nakata, K. Sugawara, R. Shimizu, Y. Okada, P. Han, T. Hitosugi, K. Ueno, T. Sato, and T. Takahashi, *NPG Asia Materials* **8**, e321 (2016).
- [24] A. Mielke, *Journal of Physics A: Mathematical and General* **24**, L73 (1991).
- [25] A. Mielke, *Journal of Physics A: Mathematical and General* **25**, 4335 (1992).
- [26] A. Mielke and H. Tasaki, *Communications in Mathematical Physics* **158**, 341 (1993).
- [27] H. Tasaki, *Physical Review Letters* **69**, 1608 (1992).
- [28] H. Tasaki, *Progress of Theoretical Physics* **99**, 489 (1998).
- [29] M. Ichimura, K. Kusakabe, S. Watanabe, and T. Onogi, *Physical Review B* **58**, 9595 (1998).
- [30] S. Watanabe, M. Ichimura, T. Onogi, Y. A. Ono, T. Hashizume, and Y. Wada, *Japanese Journal of Applied Physics* **36**, L929 (1997).
- [31] K. Penc, H. Shiba, F. Mila, and T. Tsukagoshi, *Physical Review B* **54**, 4056 (1996).
- [32] P. Giannozzi, S. Baroni, N. Bonini, M. Calandra, R. Car, C. Cavazzoni, D. Ceresoli, G. L. Chiarotti, M. Cococcioni, I. Dabo, *et al.*, *Journal of physics: Condensed matter* **21**, 395502 (2009).
- [33] D. Vanderbilt, *Physical Review B* **41**, 7892 (1990).
- [34] A. Dal Corso, *Computational Materials Science* **95**, 337 (2014).
- [35] <http://people.sissa.it/~dalcorso/pslibrary/index.html>.
- [36] J. P. Perdew, K. Burke, and M. Ernzerhof, *Physical Review Letters* **77**, 3865 (1996).
- [37] M. Cococcioni and S. de Gironcoli, *Physical Review B* **71**, 035105 (2005).
- [38] N. Marzari, D. Vanderbilt, A. De Vita, and M. C. Payne, *Physical Review Letters* **82**, 3296 (1999).
- [39] See Supplemental Material for a description of spin-orbit effects and the 4x4 CDW phase. Extra Wannier functions plots are also presented.
- [40] S. Baroni, S. de Gironcoli, A. Dal Corso, and P. Giannozzi, *Reviews of Modern Physics* **73**, 515 (2001).
- [41] A. Georges, G. Kotliar, W. Krauth, and M. J. Rozenberg, *Reviews of Modern Physics* **68**, 13 (1996).
- [42] <http://amulet-code.org/>.
- [43] E. Gull, A. J. Millis, A. I. Lichtenstein, A. N. Rubtsov, M. Troyer, and P. Werner, *Reviews of Modern Physics* **83**, 349 (2011).
- [44] N. Marzari and D. Vanderbilt, *Physical Review B* **56**, 12847 (1997).
- [45] N. Marzari, A. A. Mostofi, J. R. Yates, I. Souza, and D. Vanderbilt, *Reviews of Modern Physics* **84**, 1419 (2012).
- [46] A. A. Mostofi, J. R. Yates, G. Pizzi, Y.-S. Lee, I. Souza, D. Vanderbilt, and N. Marzari, *Computer Physics Communications* **185**, 2309 (2014).
- [47] M. Pizzochero and O. V. Yazyev, *Physical Review B* **96**, 245402 (2017).
- [48] S. Tongay, H. Sahin, C. Ko, A. Luce, W. Fan, K. Liu, J. Zhou, Y.-S. Huang, C.-H. Ho, J. Yan, *et al.*, *Nature communications* **5**, 3252 (2014).
- [49] A. M. Woolley and G. Wexler, *Journal of Physics C: Solid State Physics* **10**, 2601 (1977).
- [50] S.-K. Chan and V. Heine, *Journal of Physics F: Metal Physics* **3**, 795 (1973).
- [51] W. L. McMillan, *Physical Review B* **12**, 1187 (1975).
- [52] W. L. McMillan, *Physical Review B* **14**, 1496 (1976).
- [53] V. I. Anisimov, J. Zaanen, and O. K. Andersen, *Physical Review B* **44**, 943 (1991).
- [54] M. Itoh, M. Tsuchiya, H. Tanaka, and K. Motoya, *Journal of the Physical Society of Japan* **68**, 2783 (1999).
- [55] A. S. Erickson, S. Misra, G. J. Miller, R. R. Gupta, Z. Schlesinger, W. A. Harrison, J. M. Kim, and I. R. Fisher, *Physical Review Letters* **99**, 016404 (2007).
- [56] F. Pollmann, P. Fulde, and K. Shtengel, *Physical Review Letters* **100**, 136404 (2008).
- [57] A. Tanaka and H. Ueda, *Physical Review Letters* **90**, 067204 (2003).
- [58] R. Chisnell, J. Helton, D. Freedman, D. Singh, R. Bewley, D. Nocera, and Y. Lee, *Physical Review Letters* **115**, 147201 (2015).
- [59] X.-L. Yu, D.-Y. Liu, Y.-M. Qian, J. Wu, H.-Q. Lin, K. Chang, and L.-J. Zou, *Physical Review B* **96**, 125138 (2017).
- [60] A. S. Nngan, S. K. Mahatha, K. Guillo, M. Bianchi, C. E. Sanders, K. Hanff, K. Rossnagel, J. A. Miwa, C. Breth Nielsen, M. Bremholm, and P. Hofmann, *Physical Review B* **96**, 195147 (2017).
- [61] A. Ribak, I. Silber, C. Baines, K. Chashka, Z. Salman, Y. Dagan, and A. Kanigel, *Physical Review B* **96**, 195131 (2017).
- [62] Y. Iqbal, W.-J. Hu, R. Thomale, D. Poilblanc, and F. Becca, *Physical Review B* **93**, 144411 (2016).
- [63] M. Calandra, *ArXiv e-prints* (2018), arXiv:1803.08361 [cond-mat.mtrl-sci].